The transport and fate of riverine fine sediment exported to a semi-open system

Philippe Delandmeter[a,*], Stephen Lewis[b], Jonathan Lambrechts[a], Eric Deleersnijder[c,d], Vincent Legat[a], Eric Wolanski[b]

[a] *Université catholique de Louvain, Institute of Mechanics, Materials and Civil Engineering (IMMC), Avenue Georges Lemaître 4, B-1348 Louvain-la-Neuve, Belgium*
[b] *Catchment to Reef Research Group, TropWATER, James Cook University, Townsville QLD 4811, Australia*
[c] *Université catholique de Louvain, Institute of Mechanics, Materials and Civil Engineering (IMMC) & Earth and Life Institute (ELI), Avenue Georges Lemaître 4, B-1348 Louvain-la-Neuve, Belgium*
[d] *Delft University of Technology, Delft Institute of Applied Mathematics (DIAM), Mekelweg 4, 2628CD Delft, The Netherlands*

Abstract

Understanding the transport and fate of suspended sediment exported by rivers is crucial for the management of sensitive marine ecosystems. Sediment transport and fate can vary considerably depending on the geophysical characteristics of the coastal environment. Fine sediment transport was studied in a setting in between "open" (uninterrupted coasts) and "semi-enclosed" (bays) coastal systems, namely a "semi-open" system of shallow coastal water with long ($\sim$ 20 km) stretches of open coasts separated by capes and headlands. The case study was the large, seasonal, Burdekin River that discharges to a wide continental shelf containing headlands and shallow embayments adjacent to the Great Barrier Reef, Australia. A new three-dimensional fine sediment module for the unstructured-mesh SLIM 3D hydrodynamic model was developed. The model was successfully validated against available field data. The results were compared to previous studies on the Burdekin River sediment transport and differences were analysed. Wind direction and speed during river floods largely control the dynamics and the fate of the fine sediment. Most (67% for 2007) of the riverine fine sediment load is deposited near the river mouth; the remaining sediment is transported further afield in a riverine freshwater plume; that sediment can reach sensitive marine ecosystems and should be a priority for management. Dur-

*Corresponding author
Email address: philippe.delandmeter@uclouvain.be (Philippe Delandmeter)

ing the rest of the year, when the river flow has ceased, wind-driven resuspension events redistribute the deposited sediment within embayments but generate negligible longshore transport. This study suggests that semi-open systems trap most of the riverine fine sediment, somewhat like semi-enclosed systems.

Keywords: fine sediment transport, semi-open system, settling and resuspension, Burdekin River in the Great Barrier Reef, SLIM 3D, unstructured mesh

1. Introduction

Increased loads of riverine suspended sediment due to watershed development (Syvitski et al., 2005; Milliman and Farnsworth, 2011) cause considerable impacts on sensitive marine ecosystems including coral reefs (Fabricius, 2005; Bartley et al., 2014) and seagrass meadows (Restrepo et al., 2006). These impacts include sedimentation (Weber et al., 2012; Flores et al., 2012; Cabaço et al., 2008), elevated turbidity reducing photic depth (Fabricius et al., 2005, 2013, 2014; Petus et al., 2014), and stressors associated with pollutants attached to sediment such as nutrients, pesticides and trace metals (Weber et al., 2006; Harrington et al., 2005).

The understanding of the delivery, transport and final fate of terrestrial sediment is crucial to predict the impacts of sediment on marine ecosystems. The fate of riverine sediment exported to the ocean depends on the width and depth of the continental shelf, the presence of an offshore canyon and the geomorphology of the coastline. The different regions can be differentiated between open and semi-enclosed systems. In open systems the exported river sediment moves long distances (hundreds to thousands of kilometres) along or across the continental shelf. In these cases, the fate of the sediment exported from the river is influenced by the offshore bathymetry. For example, the Eel (Puig et al., 2003, California) and Sepik (Kuehl et al., 2004, Papua New Guinea) Rivers discharge sediment across a narrow and steep shelf, where this sediment is then transported through a canyon to the deep ocean. In contrast, the Yangtze (Liu et al., 2007), Amazon (Froidefond et al., 1988) and Mekong (Xue et al., 2010) Rivers discharge to a wide and shallow shelf where the sediment is transported longshore by coastal currents and is largely deposited close to the coastline, but far from the river mouth. For semi-enclosed systems such as the La Sa Fua River (Wolanski et al., 2003, Guam), nearly 100% of the river sediment is deposited into a sheltered embayment near the mouth, although large storms (i.e. typhoons) can flush sediment out of the bay. Somewhere in between open and semi-enclosed systems, one defines semi-open systems, where the open coast is cut by numerous capes and headlands. The bays are more open to the sea than in semi-enclosed systems. There is consequently more interaction between the bays and the open sea. But the

capes and headlands prevent coastal currents from transporting the sediment long distances. An example of such a system is the Great Barrier Reef (GBR), where riverine sediment is discharged to a wide and shallow continental shelf containing numerous headlands and embayments. The sediment transport and fate in such a system are less well understood.

The Burdekin River (Fig. 1) is the largest supplier of suspended sediment to the Great Barrier Reef off north-eastern Australia with an average annual contribution of approximatively 4 Mt (1 Mt is 10^9 kg) per year, or 28% of the total sediment export to the GBR (Kroon et al., 2012). Burdekin River sediment loads have increased by a factor of 5 to 10 since European settlement (∼1850) (Bartley et al., 2014). The annual loads are highly variable from year to year, due to the rainfall variability in its dry tropical watershed, with a range from $4 \cdot 10^{-3}$ to 15 Mt per year, between 1987 and 2010 (Kuhnert et al., 2012). A recent study found a significant relationship between Burdekin discharge, total phosphorus and suspended sediment loads with photic depth in Cleveland Bay (Fabricius et al., 2014), implying that the river has a considerable influence on the health and biodiversity of coral reefs (Roff et al., 2013; Clark et al., 2014) and seagrass meadows (Devlin et al., 2013; Petus et al., 2014) in the region. Indeed, several studies have shown that land use change and climatic variability in the Burdekin catchment are recorded in coral cores (Isdale et al., 1998; McCulloch et al., 2003; Hendy et al., 2003; Lewis et al., 2007; Lough, 2007).

The vast majority of suspended sediment exported from the Burdekin River is delivered during elevated flow conditions of short duration (i.e. commonly a few weeks) which coincide with NE Australia's summer wet season (December to April). These elevated Burdekin River flows form freshwater plumes in the GBR lagoon which can be traced hundreds of kilometres from the river mouth (King et al., 2001; Devlin and Brodie, 2005). While the movements of freshwater and suspended sediment in Burdekin flood plumes have been well documented (Wolanski and Jones, 1981; Wolanski and van Senden, 1983; Devlin and Brodie, 2005; Bainbridge et al., 2012), the fate of the newly delivered suspended sediment is disputed.

Sediment budgeting work initially suggested that the majority of suspended sediment loads (∼ 90%) delivered from the Burdekin River was primarily deposited close to the river mouth (Devlin and Brodie, 2005; Bainbridge et al., 2012) before being resuspended and moved hundreds of kilometres northward and longshore with the prevailing coastal wind-driven currents into Bowling Green, Cleveland and Halifax Bays (Woolfe and Larcombe, 1998; Orpin et al., 2004). However, recent research using newly collected and dated sediment cores has challenged this hypothesis and concluded that "very little" sediment delivered from the Burdekin River moves past Upstart Bay (Lewis et al., 2014). Under this scenario, most of the sediment transport

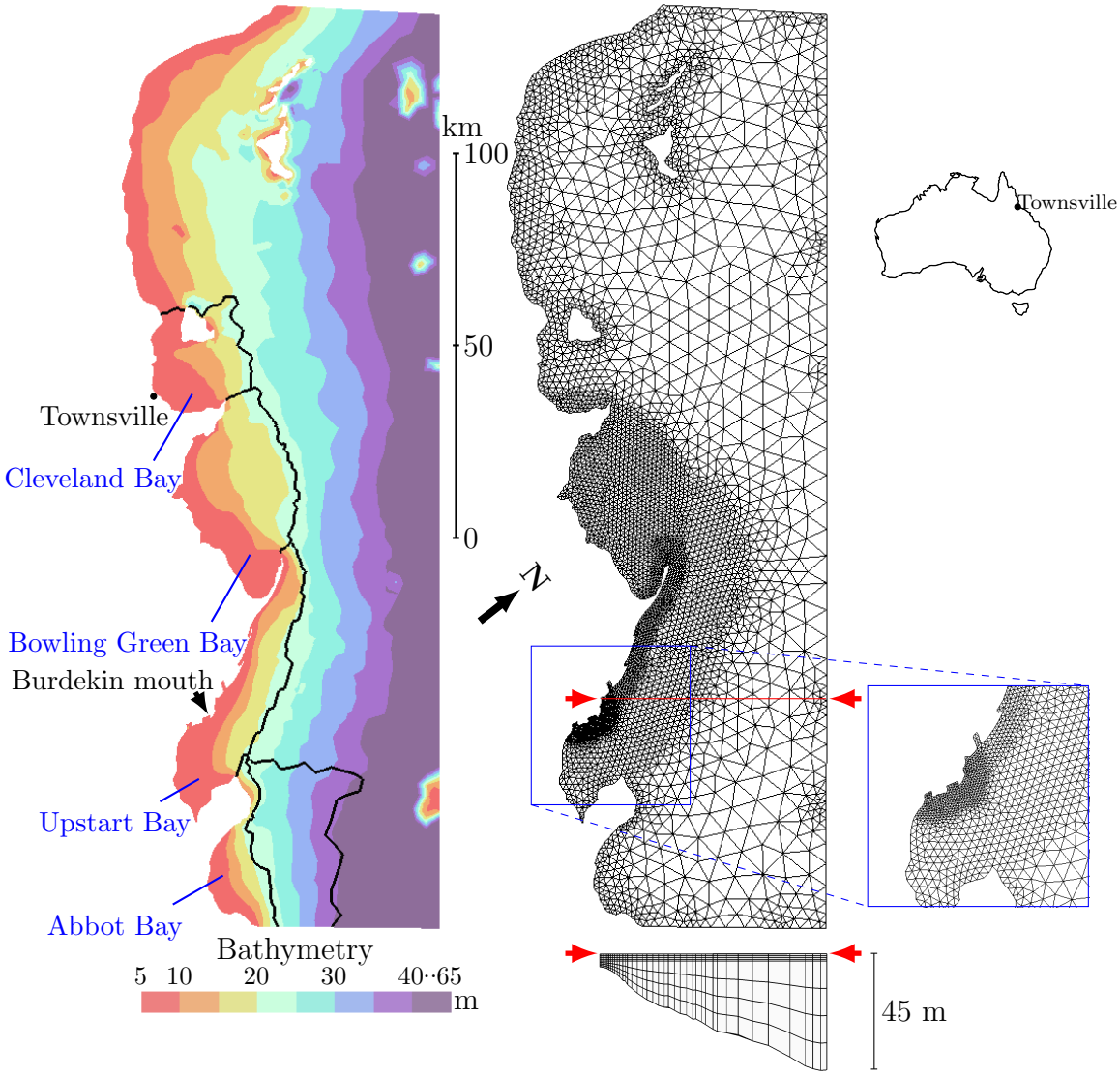

Fig. 1: Burdekin Region. Left: In order to compute sediment budgets, five zones were defined: Upstart, Bowling Green, Cleveland and Abbot Bays, and the middle-shelf offshore Abbot Bay. Right: Unstructured Mesh used by SLIM 3D: top view (top) and vertical cut (bottom). The mesh was discretized into $\sim$ 8,000 horizontal elements and extruded in 8 vertical layers. The mesh horizontal resolution is increased close to the coastline, in shallow waters, and in Upstart and Bowling Green Bays. The first four top vertical layers have a constant depth, the others are adapted to the bathymetry as σ-layers.

outside Upstart Bay occurs during times of high river discharge. These conflicting conclusions considerably influence the management strategies for controlling sediment erosion in the Burdekin watershed as the emphasis for catchment prioritisation needs to be placed on the sediment that moves longer distances and has the potential to impact sensitive marine ecosystems (Bartley et al., 2014). Specifically, if the sediment that is transported past Upstart Bay occurs only during large river flow events, then the subsequent long shore drift process becomes unimportant, and management should target the fine ($< 15.6\,\mu m$) organic rich material that travels large distances in Burdekin River flood plumes (Bainbridge et al., 2012). Hence the key research questions are as follows: where is the suspended sediment discharged from the Burdekin River deposited in the marine environment and when does this occur?

This study used numerical modelling to examine the delivery, transport and fate of suspended sediment delivered from the Burdekin in the 2007 calendar year. Section 2 describes the numerical model used in this study: SLIM 3D, and details the different data used. Section 3 validates the model, explains the sediment transport process and gives the budget of the sediment delivered by the Burdekin River. These results are discussed in Section 4 before concluding in Section 5.

2. Methods

2.1. Numerical modelling

SLIM 3D[1] is a baroclinic discontinuous Galerkin finite element model for coastal flows (Kärnä et al., 2013; Blaise et al., 2010; Comblen et al., 2010). This model enables the use of unstructured grids, which greatly enhances the quality of simulations in the case of a domain with complex topography and large velocity and density variations, such as the Burdekin region. The physical equations dealt with and the parametrizations used are detailed in Appendix A.1. SLIM 3D has already been applied to the Rhine River plume, in an idealised set up (Kärnä et al., 2013). However, it has never been used in such a complex region. 2D sediment module coupled with the 2D version of SLIM has already been used in many studies (Lambrechts et al., 2010; Gourgue et al., 2013; Elskens et al., 2014; de Brauwere et al., 2014; Pham Van et al., 2014), but there was no 3D sediment module in SLIM 3D before this study.

The fine sediment module is the 3D extension of the 2D module used by Lambrechts et al. (2010) in a study of the sediment budget in Cleveland Bay, NE Australia. The key aspects of this model of flocculating fine sediment are as follows (Fig. 2):

[1]Second-generation Louvain-la-Neuve Ice-ocean Model (`www.climate.be/slim`)

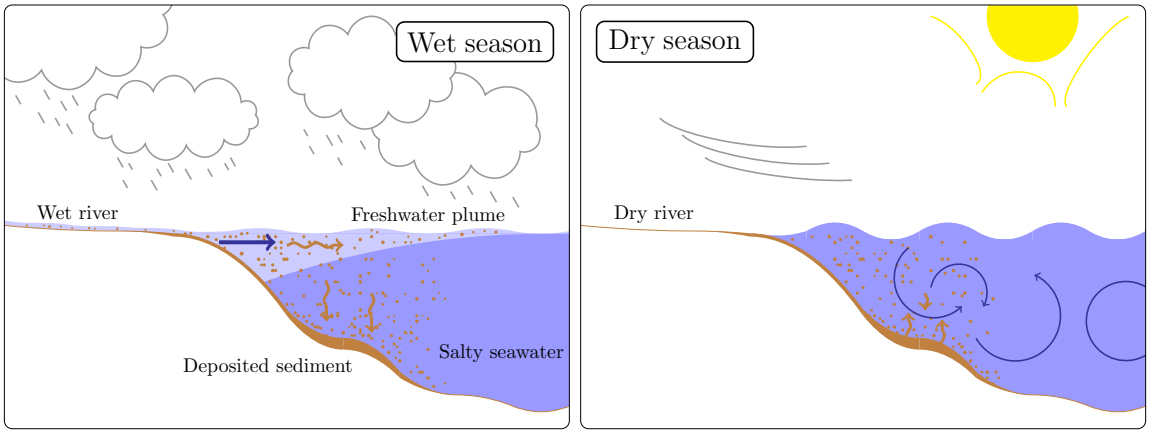

Fig. 2: Schematic representation of the processes involved in the transport of the sediment: flood event during wet season (left) and resuspension event during dry season (right).

1. The suspended sediment concentration is represented as a passive tracer that is transported by the water currents. At the open boundaries, sediment leaves the domain with currents pointing outward, but there is no inflow of sediment with currents pointing inward.
2. Over the whole domain, a vertical settling velocity is added to the hydrodynamical vertical velocity. This velocity is proportional to the sediment concentration, as it is characteristic of cohesive sediment (Lambrechts et al., 2010). The sediment plume is then much smaller than the freshwater plume.
3. At the bottom boundary, i.e. on the sea floor, the suspended sediment can settle to become deposited sediment if the weather conditions are calm. Otherwise, the deposited sediment erodes to become suspended sediment. This erosion is due to either wave induced fluidisation of the mud, or entrainment.

Model equations are detailed in Appendix A.2. The sediment model is sensitive to key parameters such as the settling velocity. In this study, the parameters are directly adapted from those of Lambrechts et al. (2010), which were calibrated in the same region (Cleveland Bay).

In order to draw budgets and analyse the proportion of suspended and deposited sediment in the different bays, the region was divided into the five following zones: Upstart, Bowling Green, Cleveland and Abbot Bays (Fig. 1), extending to the 22 m isobath (Larcombe and Carter, 2004; Belperio, 1983), where the majority of the terrigenous sediment deposition and resuspension occurs (Orpin et al., 1999), and the middle-shelf region offshore Abbot Bay extending from the 22 m to the 40 m isobath.

The region was discretized into $\sim$ 8,000 triangular elements, whose size varies between 500 m and 7 km. The horizontal mesh size is a function of the distance to the coast and the bathymetry: the closer to the coast and the shallower, the thinner the mesh. Moreover, the resolution is increased in Upstart and Bowling Green Bays, where the sediment was expected to go. Those horizontal elements were extruded to build 8 vertical layers in all the domain. In order to resolve correctly the freshwater plume, the vertical discretization is thinner close to the surface. The first four top layers are at constant depth, which is important to preserve the vertical profile of the plume. The next four layers are adapted to the bathymetry as σ-layers. The four thin top layers are necessary to resolve correctly the plume dynamics. Without them, the plume would be too thick and would not extend far enough from the river mouth. The bottom layers have a coarser resolution in deeper areas. However the sediment is not deposited in the deepest regions where the vertical resolution is the worst. The loss of resolution in mid-depth regions where sediment is deposited does not seem to affect the results. Therefore the 3D mesh has $\sim$ 65,000 prismatic elements (Fig. 1). The horizontal mesh was generated using GMSH software (Geuzaine and Remacle, 2009).

2.2. Data acquisition

To either run the model or validate the simulation results, various data were necessary. This section gives details on the data used in this study.

Bathymetry. The bathymetry is a smoothed linear interpolation from the Project 3DGBR dataset, with a resolution of 100 m (Beaman, 2010). The smoothing was achieved with a diffusion operator. It removed the unresolved features of the bathymetry. The error introduced by this operation was smaller than 5% on more than 97% of the domain. Error was mainly introduced at the reefs close to the north-east open boundary.

Wind. Wind data were taken from the NCEP Climate Forecast System Reanalysis (Saha et al., 2010), with a temporal resolution of 6 hours, and a spatial resolution of $0.3° \times 0.3°$. The wind shadow observed downwind in the Cleveland, Bowling Green and Upstart Bays are not resolved in these data. Wind shadows of 8 km were added to NCEP wind data in order to reproduce the pattern of wind resuspension observed in the data. The main winds in this region are the trade winds, blowing from the south-east. While they generally do not exceed $5\,\mathrm{m\,s^{-1}}$, they can occasionally reach more than $10\,\mathrm{m\,s^{-1}}$.

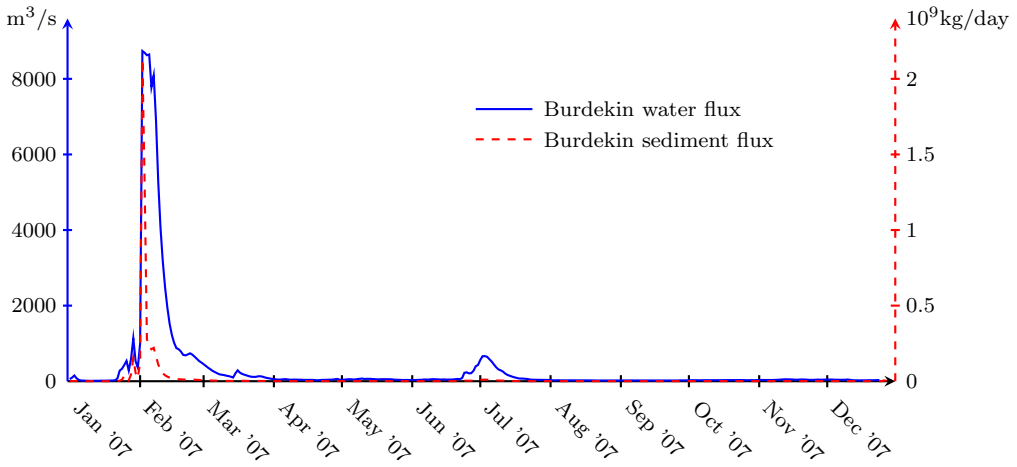

Fig. 3: Burdekin River water and sediment discharge at Clare station for 2007. In blue: volumetric flow rate (with scale on the left); in dashed red: river sediment flux (with scale on the right).

Tides. At open sea boundaries, tidal forcing was applied using the OSU TOPEX/ Poseidon Global Inverse Solution TPXO 7.2 dataset (Egbert and Erofeeva, 2002), with a spatial resolution of 1/4°. The tidal range in the region is about 3m.

Burdekin river flow and sediment loads. The water flow discharged at the Burdekin River mouth was forced using the daily data measured at the 120006B Clare station, 40 km upstream from the river mouth (DNRM, 2014). The volumetric flow rate was under $100\,\mathrm{m^3\,s^{-1}}$ most of the year, except for a large flood event in February, during which the flow rate exceeded $8000\,\mathrm{m^3\,s^{-1}}$ (Fig. 3). A much smaller wet event occurred in July. The sediment concentration at the river was imposed using data collected at Inkerman Bridge, $\sim$ 26 km downstream of Clare Station (Bainbridge et al., 2007) (Fig. 3). The load of sediment discharged by the river in 2007 is typical of an average year ($\sim$ 6 Mt). Every year, the river is almost dry all the time except for a big flood event during summer.

Photic depth. The photic depth is a measure of water clarity. The fine sediment concentration predicted by the model was compared with photic depth data determined from satellite observation (Weeks et al., 2012), with a spatial resolution of $1\,\mathrm{km} \times 1\,\mathrm{km}$. The photic depth was converted to sediment concentration following Wolanski and Elliott (2015): $C = 6600\ \zeta^{-1.12}$, where C is the sediment concentration (mg/l) and ζ is the photic depth (m).

Plume suspended sediment and salinity. During the flood event, sea surface suspended sediment concentration and salinity measurements were taken at various locations on February 6th and 7th, 2007 (Bainbridge et al., 2007). Those data were used for model validation.

Cyclone Yasi wind conditions. To study the transport of sediment under cyclone conditions, the wind conditions during Tropical Cyclone Yasi were used. Yasi was a category 5 tropical cyclone that struck the Burdekin region on February 3rd, 2011. During three days, 10 minute-averaged wind speed was above $10\,\mathrm{m\,s^{-1}}$, and during a few hours, it was above $20\,\mathrm{m\,s^{-1}}$, blowing most of the time towards the west and north-west. Data used in this study were 10 minute-averaged wind speed measured at Hardy Reef platform, from the Australian Institute of Marine Science (AIMS, 2014). Other data necessary for the "cyclone condition" run, such as initial conditions, river flow and tides were taken running the model in April 2007 (conditions after the flood event).

2007 year data. Apart from Cyclone Yasi data, all the data were taken during the 2007 calendar year. This year was chosen because it represents well an average year and for the large amount of data available. January 1st and December 31st are the initial and end times of the simulation. This allows the model to be in regime when the flood event begins.

3. Results

3.1. Sediment dynamics quick summary

The regional hydrodynamics and sediment dynamics were simulated from January 1st, 2007 to December 31st, 2007 with SLIM 3D. The flood event began in early February. Most of the sediment (67%) settled within Upstart Bay. Driven by the northerly wind (Fig. 4), the remaining part drifted to Abbot Bay, and further away. Later, during south-easterly (SE) wind the sediment was pushed northwards along the coast. After the flood event, the sediment mass released at the Burdekin mouth was negligible. During a few subsequent SE wind events (Fig. 7), settled sediment was resuspended and pushed northwards. Part of it was deposited just to the north of Cape Bowling Green, since this region is sheltered from SE winds.

3.2. Flood season modelling results

Fig. 4 shows the comparison between the simulation results and satellite images of the plume during the flood event of February 2007. At this time, a slight northerly wind (3-5 $\mathrm{m\,s^{-1}}$) pushed the plume southward. For February 11, vertical cuts of the

simulated sediment concentration and salinity are shown on Fig. 5. The model closely matched the outer extent of the flood plume, although the finer-scale features of the primary plume (i.e. close to the river mouth) shown by the true color satellite image were not reproduced by the model (Fig. 4). The true color satellite image did not provide a quantitative measure of salinity or suspended sediment concentration. The measurements of sediment concentration and salinity from the surface of the plume compared reasonably well with those produced by SLIM 3D with some exceptions (Fig. 6). The latter occurred mostly near the river mouth where measured suspended sediment concentrations and salinity were highly variable.

There is no data about the vertical distribution of salinity and suspended sediment. However, a wrong vertical salinity profile would perturb the horizontal plume velocity, which in turn would deteriorate the sea surface salinity and sediment concentration. Similarly correct deposition areas could not be obtained without a plausible vertical sediment distribution. Moreover, the salinity and sediment concentration vertical distributions presented on Fig. 5 are in qualitative agreement with the 2011 Burdekin Plume samples presented in Bainbridge et al. (2012): beyond 11 km from the river mouth, the salinity plume is still clearly marked, with a large difference between the surface and 5 m depth salinity. The sediment roughly follows the salinity dynamics for the first 9 km but is mixed on the vertical from the 11th km.

3.3. Dry season modelling results

Under the larger resuspension events which occurred in 2007, SLIM 3D outputs were comparable to the processed photic depth data. In particular the model was able to reproduce the width and magnitude of the sediment resuspension event that occurred during the strong SE (the prevalent winds in the region) winds (10 m s^{-1}) on April 8-10 (Fig. 7 (left)) as well as several other SE wind events that occurred in 2007 (similar to Fig. 7 (left), not shown.). The model performed reasonably well for a comparatively weaker northerly wind ($\sim$ 5 m s^{-1}) which occurred in October (Fig. 7 (right)).

3.4. Global sediment budget

The model computed the fate of the 6 Mt of suspended sediment delivered from the Burdekin River in 2007. The model predicted that 86% of the suspended sediment load delivered by the Burdekin River was deposited within the modelling domain, with another 2% of the load remaining in suspension in the area. The remaining 12% of the load left the modelling domain through the open boundaries. 67% of the load delivered from the Burdekin was deposited and retained within Upstart Bay. The remaining deposited sediment load occurred in Abbot Bay, on the inner-shelf

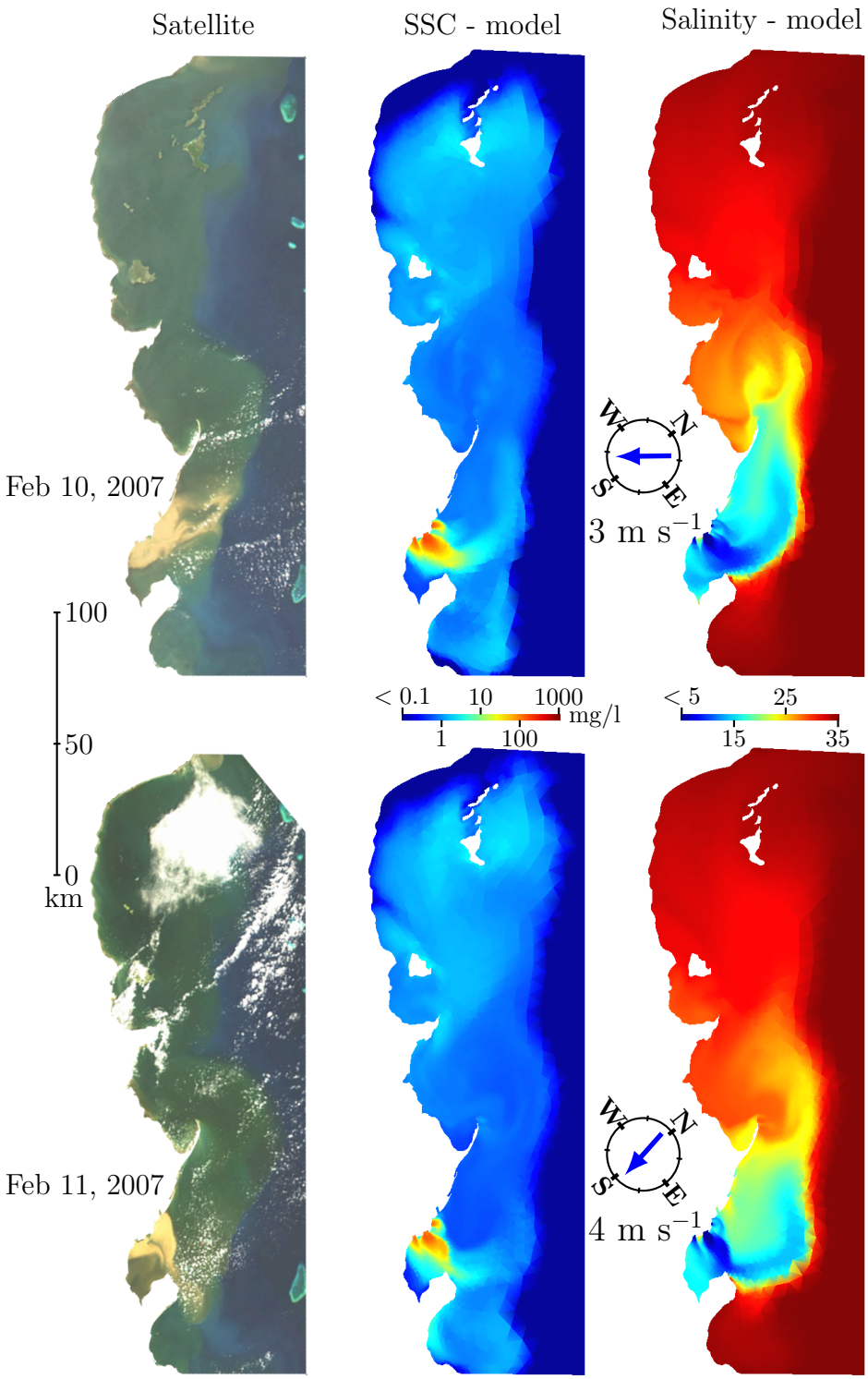

Fig. 4: Comparison between true color satellite images, sea surface suspended sediment concentration (SSC) and sea surface salinity during the flood event on February 10 (top) and February 11 (bottom). Wind speed and direction are shown in the compass.

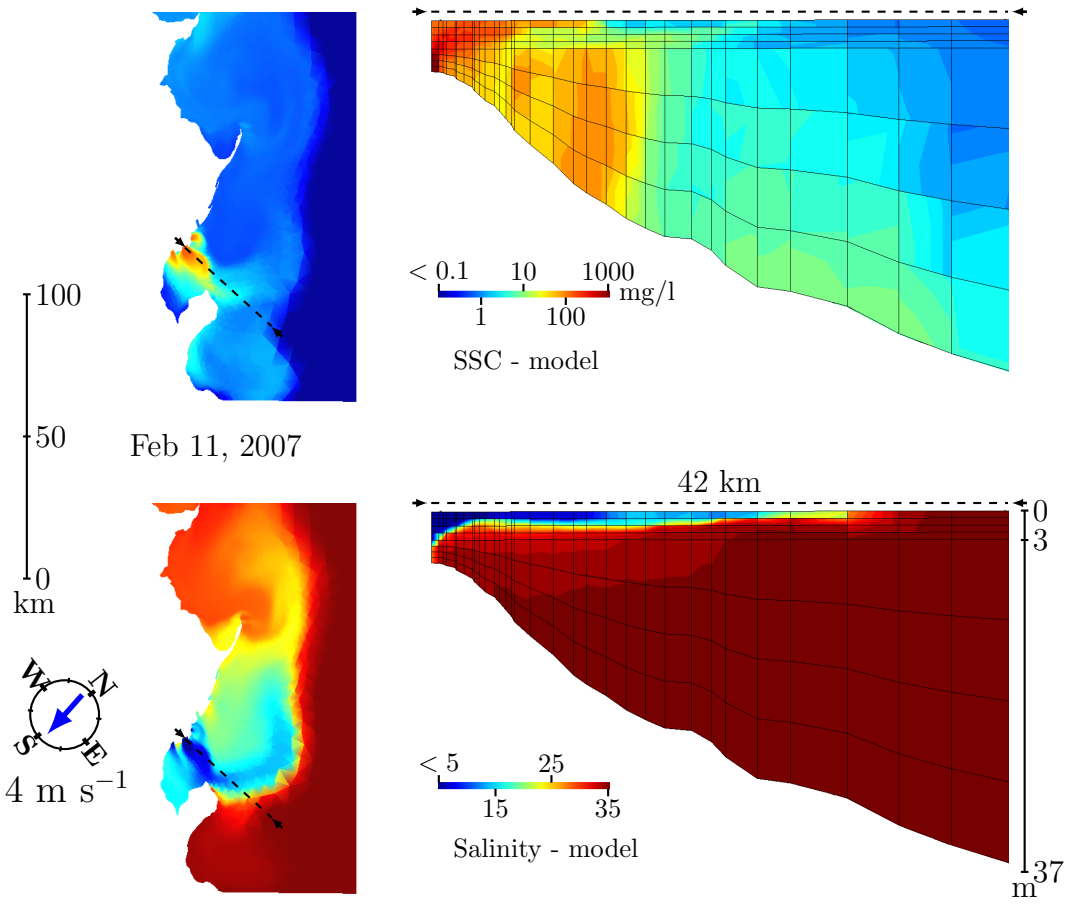

Fig. 5: Vertical cut of suspended sediment concentration (top) and salinity (bottom) for the flood event on February 11 (same event as that represented at the bottom of Fig. 4). Left: sea surface suspended sediment concentration and salinity, respectively. The cut location is illustrated with a dashed line. Right: vertical cuts. Wind speed and direction are shown in the compass.

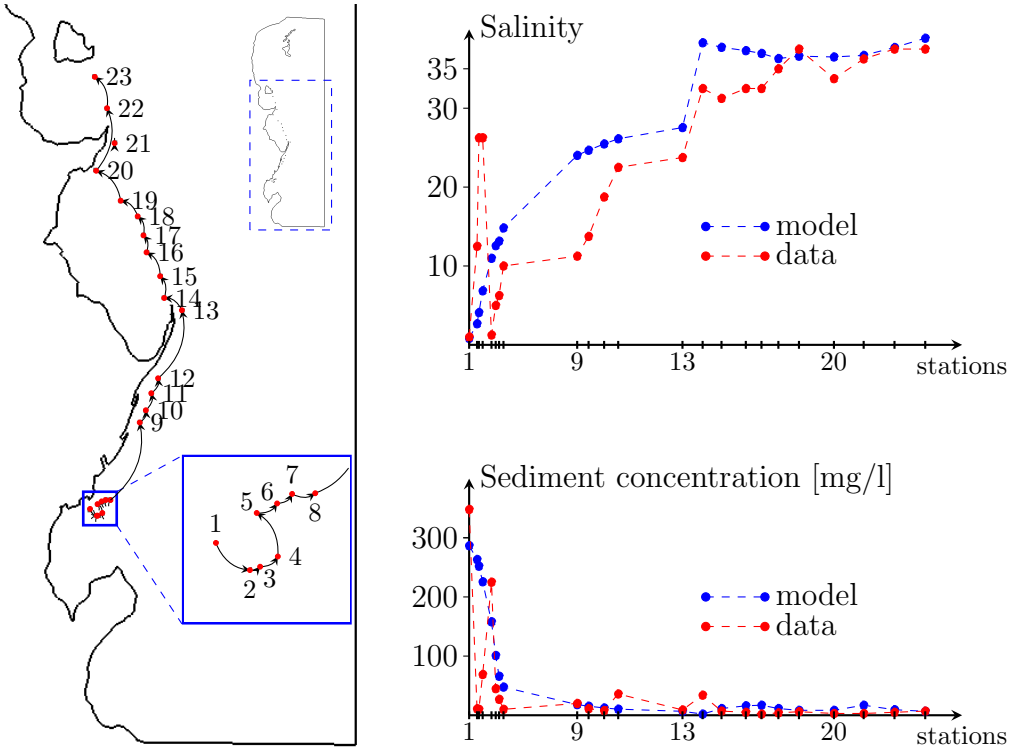

Fig. 6: Comparison between measured (Bainbridge et al., 2007) and simulated sea surface salinity and suspended sediment concentration. The map on the left shows the location of the points where measurements were taken between Feb 6 and 7 (See Table B.4 in Appendix B for details on the measure locations and time). On the right, the model and data are compared for sea surface salinity (top) and sea surface sediment concentration (bottom).

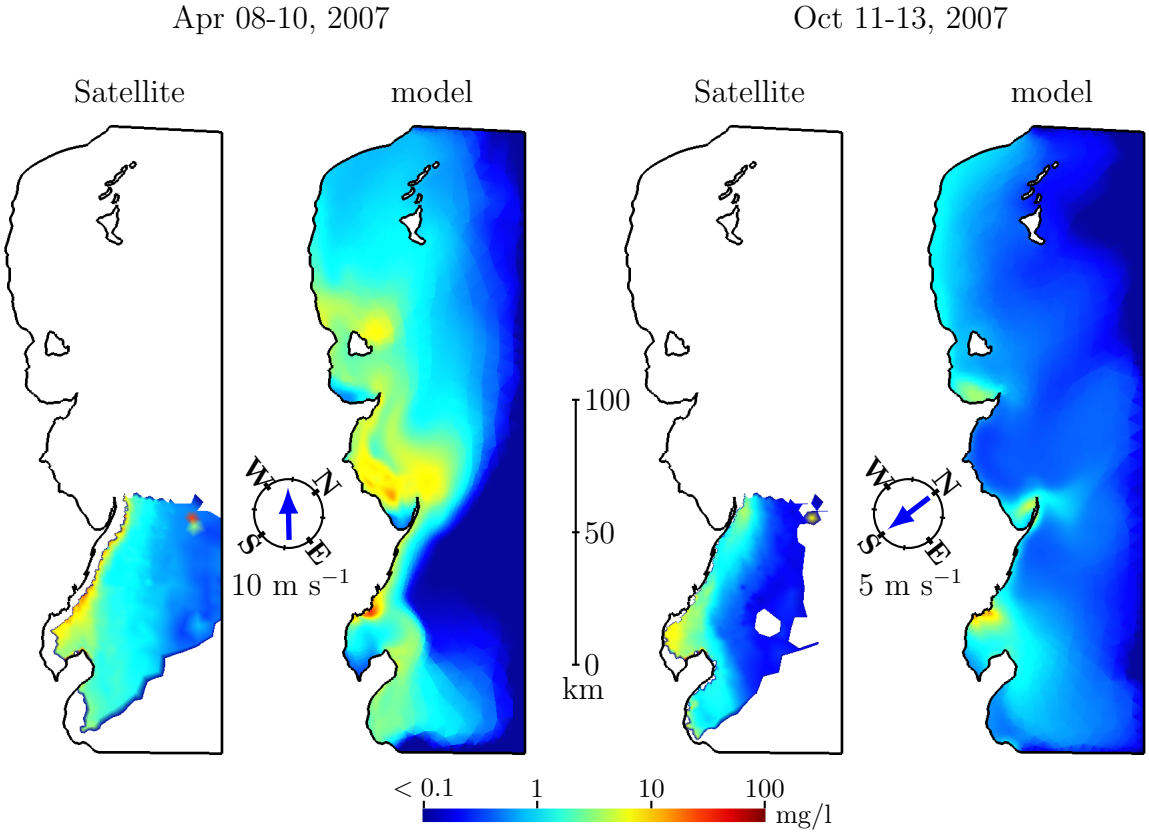

Fig. 7: Comparison between surface sediment concentration from processed satellite data (1st and 3rd map) and SLIM 3D simulation (2nd and 4th map) for the April 8-10 period (left) and the October 11-13 period (right), respectively. Satellite data are shown where available. Wind speed and direction are shown in the compass.

(6%) and the middle-shelf (7%), Bowling Green (5%) and Cleveland (0.09%) Bays (Fig. 8 (top)). 1% of the sediment was deposited in the domain outside one of the five previously defined zones.

The sediment deposited in the bays was infrequently resuspended during strong wind events in the dry season when the river flow was negligible (Fig. 8 (bottom)). During these wind-driven resuspension events, the sediment was not transported from bay to bay, but was slightly redistributed within the bays. The sediment accumulation from the 2007 Burdekin discharge event varied between 10 and 50 mm at the mouth of the Burdekin River in Upstart Bay (Fig. 9 (right)), and varied between 1 and 3 mm offshore near Cape Bowling Green. Deposition up to 1 mm in thickness was modelled to have occurred in parts of Abbot Bay.

3.5. Sediment transport under cyclone conditions

Fig. 10 shows the comparison between the deposited sediment prior to and after tropical cyclone Yaso. The results show all the deposited sediment left Abbot Bay: 99.9% of the deposited sediment in the inner-shelf part of the Bay left it, and 79% left the middle-shelf part of the Bay. The sediment from Upstart Bay was pushed northwards along the coast, and around 20% of if moved to Bowling Green Bay, where most (75%) of it remained in suspension at the end of simulation, and 25% was redeposited north of Cape Bowling Green, in a similar area to the main depositional zone in this bay.

4. Discussion

4.1. Model

The flood event was reliably simulated by SLIM 3D. The model was verified reasonably well with both the satellite data from the 10-11th of February and the suspended sediment concentration and salinity dataset from the 6-7th of February (Figs. 4 and 6). The plume is driven by the vertical salinity profile and the sediment deposition and resupension fluxes at the bottom are functions of the sediment vertical distribution. Those two vertical features, essential to understand the sediment dynamics, are captured explicitly while more parametrisations would be required in a 2D model. In this semi-open system the use of an unstructured grid was necessary to increase the resolution in the deposition areas and to capture the coastlines. The discontinuous Galerkin finite element approach allowed for an accurate modelling of the transport processes and an easy implementation on a parallel computer cluster.

However, the model could not reproduce the fine small-scale features observed, particularly close to the river mouth. But the spatial and temporal resolution of

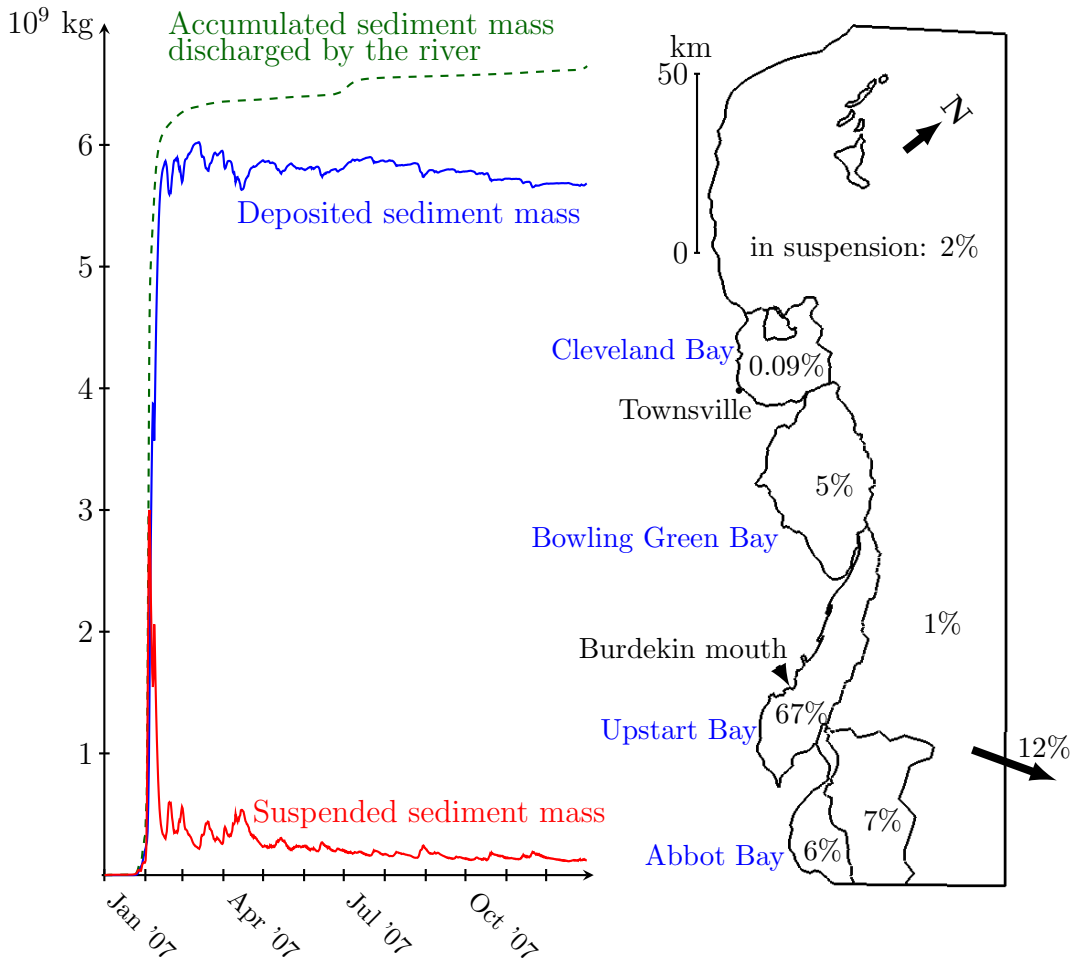

Fig. 8: Burdekin River sediment mass budget. Left: in blue: total mass deposited on the sea bed in 2007; in red: total suspended sediment mass. The brown dashed line represents the accumulated sediment mass released by the Burdekin River. Right: map of the sediment budget distribution at the end of the year. Except for the 2% which are still in suspension and the 12% which left the modelling domain, all the numbers refer to deposited sediment.

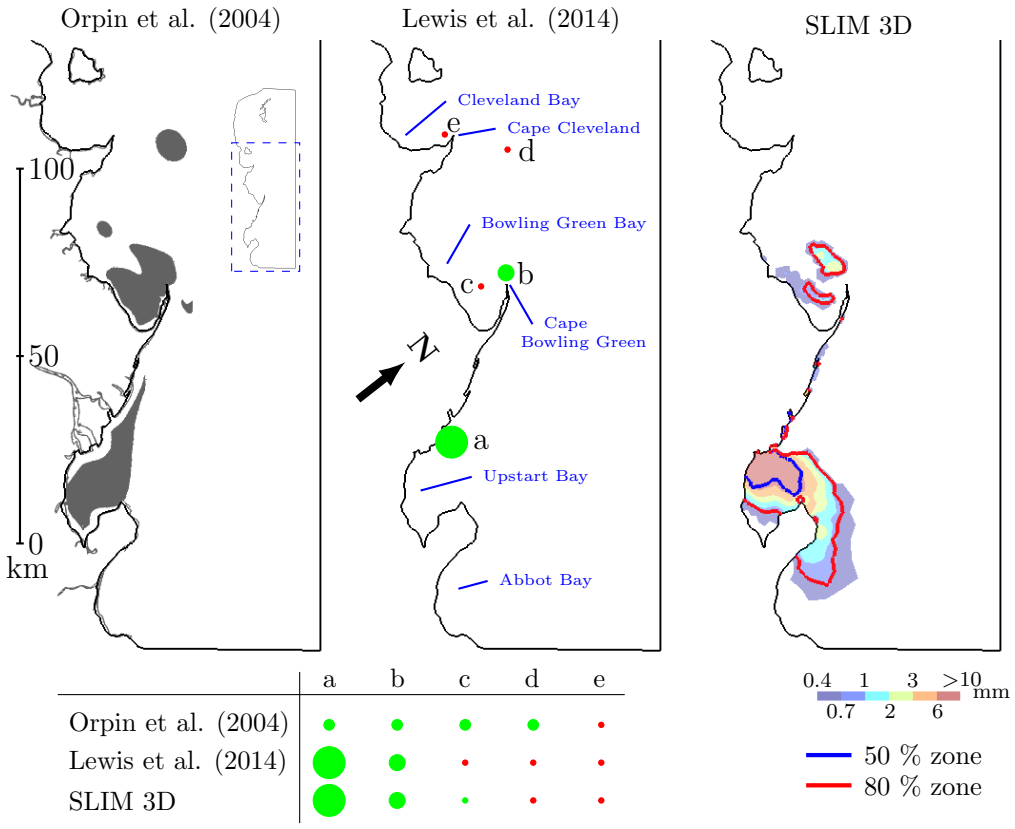

Fig. 9: Deposited sediment at the end of year 2007 modelled by SLIM 3D, and compared to core data from Orpin et al. (2004) and Lewis et al. (2014). On the left map, the grey zone represents the deposition region defined by Orpin et al. (2004). On the central map, five sediment accumulation rates have been measured by Lewis et al. (2014) (points 'a' to 'e'). Large green circles represent high accumulation rates, medium green circles represent smaller rates and red circles represent negligible rates. On the right map, the thickness of the sediment deposit at the end of 2007 is shown, and blue and red lines represent the boundary of the zones where 50% and 80% of the sediment is deposited, respectively. The table compares the deposition areas of the three studies (the size of the circles for Orpin et al. (2004) is subjective, since accumulation rate is not quantified).

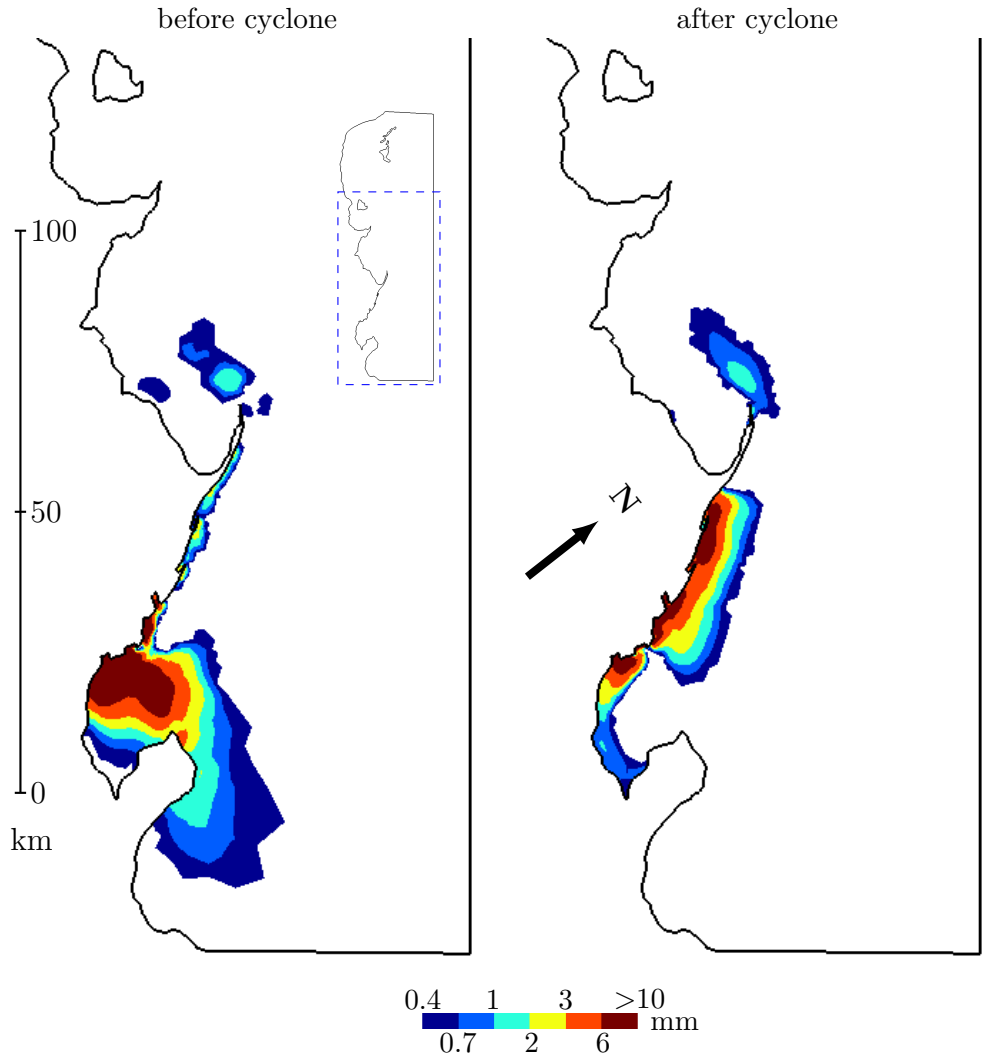

Fig. 10: Cyclone effect on sediment fate. Situation prior to (left panel) and after (right panel) the cyclone, respectively.

flood plumes are highly dynamic: large changes in salinity and suspended sediment concentration can occur over a scale of a few metres, i.e. a length scale that the model cannot resolve. Furthermore, the river discharge can also change rapidly in time and hence the daily resolution used in the data input to the model would not be able to capture those changes. Despite these fine scale discrepancies, which cannot be avoided using a model at this scale, SLIM 3D performed very well in characterising the salinity and suspended sediment dynamics in the flood plume over the period examined.

4.2. Burdekin sediment dynamics

The model showed that during the dry season, when river flow is negligible, strong winds are necessary to resuspend and transport sediment in coastal waters. It suggested that sediment fluxes from bay to bay are negligible. The finding that 67% of the 6 Mt of suspended sediment delivered in the 2007 flow event remains in Upstart Bay provides the first quantification of the partitioning and fate of sediment delivered from the Burdekin River (Fig. 8) and agrees with the assertion of Lewis et al. (2014) that "most" sediment is retained within the bay. This value is much higher than that suggested by Orpin et al. (2004) who estimated that only 10% of the Burdekin sediment load is deposited in Upstart Bay, although that study was limited by the chronology of sediment cores.

The model highlighted key depositional areas of the suspended sediment delivered from the Burdekin River that closely resemble some of the areas previously identified by Orpin et al. (2004) who collected benthic sediment grab samples (see Fig. 9 (left)). However, the model suggested that other mud-rich areas highlighted in Orpin et al. (2004), such as the southern inshore area of Bowling Green Bay and the middle of Bowling Green Bay, are currently zones of minor deposition (less than 1 mm year^{-1}). Also, the area to the east of Cape Cleveland does not appear to be a zone of current sediment deposition from the Burdekin River. Indeed a sediment core collected from this location (point 'e' on Fig. 9) only revealed a thin (7 cm) veneer of Holocene sediment (Lewis, unpublished data). Furthermore, Abbot Bay was not sampled by Orpin et al. (2004) and should be the target for further investigation based on our SLIM 3D results. The calculations of Orpin et al. (2004) are likely to be relevant over the longer Holocene period (past 7000 years), during which the Burdekin River discharged into both Bowling Green and Upstart Bays and constructed at least 13 different delta lobes (Fielding et al., 2006). However, the findings of Orpin et al. (2004) do not conform for the past 1000 years, since the Burdekin channel last avulsed to discharge into Upstart Bay, which also led to the formation of the Cape Bowling Green sand spit which now differentiates Bowling Green and Upstart Bays

(Fielding et al., 2006).

The modelling results provide clear guidance on the depositional areas for recent suspended sediment delivered from the Burdekin River and hence provide locations where the collection of sediment cores should be targeted. The accumulation rates modelled for the 2007 Burdekin River flow event matched closely with those found in the available sediment core data calculated over longer timescales (100 to 200 years, (Lewis et al., 2014)) and provide some validation of the model. Indeed, Lewis et al. (2014) measured an average accumulation rate of 25 mm year^{-1} over the past 100 years in Upstart Bay (point 'a' in Fig. 9). While the position of the sediment core (point 'a' in Fig. 9) is within a zone identified by the model to have little accumulation, it is less than 6 km from the modelled 25 mm zone. The peak discharge period in the 2007 Burdekin River flood coincided with a northerly wind which may account for this slight variation in the sediment depositional area. Maximum sediment accumulation in Bowling Green Bay occurred to the west of the tip of Cape Bowling Green and was modelled to be of the order of 1 to 3 mm. This value is lower, but of the same order of magnitude of the average accumulation in a sediment core (9 mm year^{-1} over the past 200 years: point 'b' in Fig. 9) collected from this area (Lewis et al., 2014). Accumulation rates calculated in sediment cores from the southern inshore area of Bowling Green Bay (point 'c' in Fig. 9) and the west of Cape Cleveland (point 'd' in Fig. 9) show negligible recent sediment deposition. In these areas the model suggests accumulation of less than 0.3 mm and 0.1 mm, respectively, of the sediment delivered in the 2007 Burdekin flow event.

It is noteworthy that the sediment load delivered from the Burdekin River over the past hundred years has changed with land use changes in the catchment (Lewis et al., 2007), climatic/hydrological changes (Lough et al., 2015) and dam construction (Bainbridge et al., 2014). Hence, the long-term accumulation data in the sediment cores cannot be directly compared to the modelling results for one year. The long-term loads based on ∼25 years of monitoring data (Kuhnert et al., 2012) suggest that the mean load over this time is in the order of 4 Mt, which is thought to have increased by a factor 5 to 10 since catchment modification from the 1850s; in fact the Burdekin Falls Dam constructed in 1987 traps a large proportion of sediment (Bainbridge et al., 2014) and hence the loads delivered to the end of river over a period prior to 1987 would likely have been larger than today. In that regard, the annual mean sediment loads delivered from the Burdekin River over the past hundred years are likely to be of the order of 2 to 8 Mt and so the accumulation rate data in the cores were expected to be within an order of magnitude of the modelled sediment deposition rate.

4.3. Management prioritisation

The results from SLIM 3D provide information relevant to the management prioritisation of suspended sediment delivered from the Burdekin River. Specifically the model shows that the Burdekin sediment that travels past Upstart Bay into areas of sensitive marine ecosystems such as seagrass meadows and coral reefs occur during flood plumes. Hence it is this sediment in the flood plumes that needs to be better characterised and sourced to a specific catchment area or soil type. Bainbridge et al. (2012) showed that the suspended sediment in the Burdekin flood plumes becomes more organic-rich as the plume moves past Upstart Bay and is composed of clay and fine silt material ($< 15.6\,\mu m$). While SLIM 3D cannot model the biological material formed in the plume, such as bacterial mucus and phytoplankton, it does reveal the fate of the "mineral" sediment which is likely coupled with this biological material (Bainbridge et al., 2012). Further insights into the transport and fate of suspended sediment from the Burdekin River will be gained by modelling larger flow and sediment load events as well as wind-driven resuspension events that occur at different times of the year to examine the movement and compaction potential of this newly delivered sediment. Future studies could also model different sediment types (e.g. different particle sizes and different densities) to examine if there is a compositional difference between the sediment retained within Upstart Bay and the sediment transported further afield.

4.4. Semi-open systems

The present study provides insights on the sediment deposition and fate for semi-open systems. During the wet season, most of the sediment is deposited close to the river mouth (Fig. 9). A long distance sediment transport occurs within freshwater plumes during flood events but remains limited. During the dry season, while regular wind events flush the sediment out of the exposed coastal areas, only exceptional events, such as cyclones, are able to move the sediment out of the bays (Fig. 10).

Whilst the widely accepted long-shore drift process (e.g. Woolfe and Larcombe (1998); Lambeck and Woolfe (2000); Orpin et al. (2004)) is critical for sand movement along beaches (e.g. Pringle (1986); Muller et al. (2006)) in open systems, it is unlikely to be a major process in the transport of mud-sized (< 63 µm) sediment in semi-open systems. Such systems are sheltered and differ from open settings which allow sediment to be transported hundreds to thousands of kilometres via longshore coastal wind-driven currents (e.g. Mekong and Amazon Rivers). However, those systems cannot be regarded as semi-enclosed systems, since a large fraction of the sediment mass leaves the bay of the river mouth.

5. Conclusions

SLIM 3D was used to model the transport and fate of suspended sediment delivered by a large tropical river to a semi-open system located on a shallow and wide continental shelf. The model reproduced key sediment depositional areas identified in previous studies and was able to closely reproduce the patterns and concentrations of suspended sediment and salinity measured in both the flood plume and during large resuspension events. Furthermore, the modelled sediment accumulation rates closely matched the longer-term sediment accumulation rates measured in sediment cores from the region. The model reveals that for such a system, most of the sediment is deposited and retained in the bay near the river mouth while the suspended sediment that travels longer distances is transported within freshwater plumes during flood events. Wind resuspension processes only redistribute the sediment within the embayments and do not move it from bay to bay, although the sediment is flushed out of the exposed coastal areas. Cyclones are able to move the sediment out of the bays.

It is suggested that for these semi-open systems, the management of the sediment transported long distances in the flood plumes should be the priority for protecting sensitive marine ecosystems. Future studies should examine sediment transport and fate for other similar systems with different characteristics such as a narrower or deeper shelf.

Acknowledgments

The present study was carried out in the framework of the project "Taking up the challenges of multiscale marine modelling", which is funded by the Communauté Française de Belgique under contract ARC 10/15-028 with the aim of developing and using SLIM, the Second-generation Louvain-la-Neuve Ice-ocean Model (www.climate.be/slim). Computational resources were provided by the Consortium des Équipements de Calcul Intensif (CÉCI), funded by the Belgian Fund for Scientific Research (FNRS) under Grant No. 2.5020.11. Philippe Delandmeter visited James Cook University funded by the Grant "Bourse de voyage de la Fédération Wallonie-Bruxelles". Jonathan Lambrechts is a post-doctoral researcher with the Belgian Fund for Scientific Research (FNRS). Eric Deleersnijder is an honorary research associate with the same institution. The authors want to thank Marites Canto and Eduardo da Silva for providing photic depth and true color satellite image, respectively.

Appendix A. SLIM 3D model details

Appendix A.1. Hydrodynamic model

SLIM 3D (Kärnä et al., 2013; Blaise et al., 2010; Comblen et al., 2010) solves the 3D hydrostatic Boussinesq equations. The unknowns are the following:

variable	definition
$\boldsymbol{u}$	horizontal velocity
w	vertical velocity
η	sea surface elevation
p	pressure
ρ'	density deviation
S, T	salinity and temperature

Using the notations defined in Table A.1, the equations governing the unknowns previously defined are:

$$\boldsymbol{u}: \quad \frac{\partial \boldsymbol{u}}{\partial t} + \boldsymbol{\nabla}_h \cdot (\boldsymbol{u}\boldsymbol{u}) + \frac{\partial (\boldsymbol{u}w)}{\partial z} + f\boldsymbol{e}_z \wedge \boldsymbol{u} + \frac{1}{\rho_0}\boldsymbol{\nabla}_h p = \boldsymbol{\nabla}_h \cdot (\nu_h \boldsymbol{\nabla}_h \boldsymbol{u}) + \frac{\partial}{\partial z}\left(\nu \frac{\partial \boldsymbol{u}}{\partial z}\right), \tag{A.1}$$

$$w: \quad \boldsymbol{\nabla}_h \cdot \boldsymbol{u} + \frac{\partial w}{\partial z} = 0, \tag{A.2}$$

$$\eta: \quad \frac{\partial \eta}{\partial t} + \boldsymbol{\nabla}_h \cdot \int_{-h}^{\eta} \boldsymbol{u} dz = 0, \tag{A.3}$$

$$p: \quad \frac{1}{\rho_0}\boldsymbol{\nabla}_h p = g\boldsymbol{\nabla}_h \eta + \frac{g}{\rho_0}\boldsymbol{\nabla}_h \int_z^{\eta} \rho' d\zeta, \tag{A.4}$$

$$\rho': \quad \rho' = \hat{\rho}(S,T) - \rho_0, \tag{A.5}$$

$$S: \quad \frac{\partial S}{\partial t} + \boldsymbol{\nabla}_h \cdot (\boldsymbol{u}S) + \frac{\partial (wS)}{\partial z} = \boldsymbol{\nabla}_h \cdot (\kappa_h \boldsymbol{\nabla}_h S) + \frac{\partial}{\partial z}\left(\kappa \frac{\partial S}{\partial z}\right). \tag{A.6}$$

$\hat{\rho}$ is the density state equation defined by Jackett et al. (2006). Temperature equation is similar to salinity Equation A.6. Nevertheless, in this study, the influence of temperature on density is neglected in front of salinity: density is only a function of salinity. Coriolis factor f is constant over the domain. Horizontal viscosity ν_h follows the Smagorinsky parametrization (Smagorinsky, 1963; Blaise et al., 2007),

Table A.1: Notations for the hydrodynamic model

variable	definition
f	Coriolis factor
g	gravitational acceleration
ρ_0	reference density
ν_h, κ_h	horizontal viscosity and diffusivity
ν, κ	vertical viscosity and diffusivity
x, y, z	cartesian coordinates. z is the vertical coord, varying between $-h$ and η.
h	bathymetry
$\boldsymbol{e}_z$	vertical unit vector
$\boldsymbol{\nabla}_h$	horizontal gradient operator

with parameters similar to those of Thomas et al. (2014) in their modelling of the GBR. Horizontal diffusivity κ_h is constant, with the same value as in the application SLIM 3D to an idealised setting of the Rhine region of freshwater influence (Kärnä et al., 2013). Finally, vertical eddy viscosity ν and diffusivity κ are determined from the $\kappa - \epsilon$ turbulence closure model. For this turbulence closure model, GOTM (Burchard et al., 1999), which has been coupled to SLIM 3D (Kärnä et al., 2012), is used here.

Appendix A.2. Sediment model

The sediment model is a 3D extension of the model developed by Lambrechts et al. (2010). The sediment concentration C is a passive tracer which is advected and diffused. The main unknowns are:

variable	definition
C	suspended sediment Concentration (mg l^{-1})
D	sediment Deposit concentration (mg m^{-2})
E	Erosion and deposition flux (mg m^{-2} s^{-1})

Using the variables and parameters defined in Table A.2 and A.3, the governing equations are:

$$C: \text{ On } \Omega: \frac{\partial C}{\partial t} + \boldsymbol{\nabla}_h \cdot (\boldsymbol{u} C) + \frac{\partial \big((w + w_s) C\big)}{\partial z} = \boldsymbol{\nabla}_h \cdot (\kappa_h \boldsymbol{\nabla}_h C) + \frac{\partial}{\partial z}\left(\kappa \frac{\partial C}{\partial z}\right),$$
$$\text{On } \Gamma_b: \; -\kappa \frac{\partial C}{\partial z} = E, \tag{A.7}$$

$$D: \text{ On } \Gamma_b: \frac{\partial D}{\partial t} = E, \tag{A.8}$$

$$E: \; E = a_1 \, C \, w_s \; \max\left(1 - \beta^2, 0\right) - \delta_{D>0}\Bigg(a_2 \; \max\left(\beta^4 - 1, 0\right) + a_3 \left(\frac{w}{w_0}\right)^3 \beta^4 \exp\left(-f_0 \omega^2 (H + \eta)/g - f_1\right)\Bigg), \tag{A.9}$$

where Ω is the domain and Γ_b the bottom boundary. Sediment depot D is only defined at Γ_b. At the open boundaries, sediment leaves the domain with currents pointing outward, but there is no inflow of sediment with currents pointing inward. In Equation A.9, the first term on the right hand side is the deposition flux, the second term is the erosion flux due to entrainment, and the last term is due to wave induced fluidisation of the mud.
The settling vertical velocity w_s is defined by:

$$w_s = -\delta_{w<w_0} \; \min(a_0 C, \; w_{s0}). \tag{A.10}$$

Table A.2: Notations for the equations resolved by the sediment model

variable	definition
w_s	settling vertical velocity (m s^{-1})
$\boldsymbol{w}$	wind velocity: $\boldsymbol{w} = (w_x, w_y)$ (m s^{-1})
w	wind speed: $w = \|\boldsymbol{w}\|$ (m s^{-1})
$\boldsymbol{u}_b$	bottom water velocity (m s^{-1})
u_b	bottom water speed: $u_b = \|\boldsymbol{u}_b\|$ (m s^{-1})
β	u_b/u_0
g	gravitational acceleration (m s^{-2})
$\delta_{w<w_0}$	$= 1$ is $w < w_0$, else 0
$\delta_{D>0}$	$= 1$ is $D > 0$, else 0

Table A.3: Values of the different parameters used in the sediment model

variable	definition	value
w_{s0}	settling speed threshold	$2 \cdot 10^{-4}$ m s^{-1}
w_0	wind speed threshold	10 m s^{-1}
ω	wave frequency	1.57 Hz
a_0		10^{-5} m l mg^{-1} s^{-1}
a_1		10^3 l m^{-3}
a_2		1 mg m^{-2} s^{-1}
a_3		$a_{30} + (a_{31} - a_{30}) \left(0.5 - \frac{\arctan(10\alpha)}{2\arctan(10)}\right)$
α	wind orientation factor	$\alpha = (\boldsymbol{u}_b \cdot \boldsymbol{w})/(u_b w)$
a_{30}		$6.86 \cdot 10^3$ mg m^{-2} s^{-1}
a_{31}		$3.528 \cdot 10^4$ mg m^{-2} s^{-1}
f_0		0.905
f_1		-0.0207

Appendix B. Flood data

Table B.4: Comparison between measured (Bainbridge et al., 2007) and simulated sea surface salinity and sea surface suspended sediment concentration.

Site ID	date	latitude	longitude	Salinity		SSC (mg/l)	
				data	SLIM 3D	data	SLIM 3D
1	Feb 06, 13:30	19°40.9'	147°37.5'	1	1	348	287
2	Feb 06, 14:10	19°40.6'	147°38.6'	10	2	11	263
3	Feb 06, 14:25	19°40.4'	147°38.7'	21	3	10	252
4	Feb 06, 14:40	19°39.9'	147°38.8'	21	5	69	226
5	Feb 06, 15:20	19°39.6'	147°37.6'	1	9	225	158
6	Feb 06, 15:35	19°39.1'	147°37.7'	4	10	45	101
7	Feb 06, 15:40	19°38.6'	147°37.7'	5	11	27	66
8	Feb 06, 15:55	19°38.2'	147°38.1'	8	12	10	48
9	Feb 06, 16:40	19°29.6'	147°32.7'	9	19	20	18
10	Feb 06, 16:50	19°28.2'	147°31.9'	11	20	11	15
11	Feb 06, 17:05	19°26.5'	147°30.7'	15	20	8	12
12	Feb 06, 17:25	19°24.8'	147°29.8'	18	21	36	10
13	Feb 06, 17:50	19°17.5'	147°24.9'	19	22	9	7
14	Feb 07, 7:20	19°18.2'	147°22.2'	26	31	34	2
15	Feb 07, 7:45	19°17.0'	147°19.8'	25	30	7	11
16	Feb 07, 8:13	19°16.5'	147°16.4'	26	30	5	16
17	Feb 07, 8:35	19°15.5'	147°14.4'	26	30	2	17
18	Feb 07, 8:53	19°14.7'	147°12.1'	28	29	4	11
19	Feb 07, 9:10	19°15.2'	147°9.3'	30	29	6	8
20	Feb 07, 9:30	19°15.2'	147°4.3'	27	29	3	8
21	Feb 07, 10:00	19°11.4'	147°3.0'	29	29	3	17
22	Feb 07, 10:20	19°9.7'	146°59.0'	30	30	5	9
23	Feb 07, 10:45	19°8.5'	146°54.8'	30	31	7	7

References

AIMS, 2014. Wind speed (scalar avg 10 min) at Hardy Reef. Available at http://data.aims.gov.au/aimsrtds/datatool.xhtml, last accessed on December 22, 2014.

Bainbridge, Z.T., Lewis, S.E., Brodie, J.E., 2007. Event-based community water quality monitoring in the Burdekin Dry Tropics Region: 2006-2007 (2 volumes). ACTFR Report No. 07/22 for the Burdekin Dry Tropics NRM. Technical Report. Australian Centre for Tropical Freshwater Research, James Cook University, Townsville.

Bainbridge, Z.T., Lewis, S.E., Smithers, S.G., Kuhnert, P.M., Henderson, B.L., Brodie, J.E., 2014. Fine-suspended sediment and water budgets for a large, seasonally dry tropical catchment: Burdekin River catchment, Queensland, Australia. Water Resources Research 50, 9067–9087.

Bainbridge, Z.T., Wolanski, E., Álvarez-Romero, J.G., Lewis, S.E., Brodie, J.E., 2012. Fine sediment and nutrient dynamics related to particle size and floc formation in a Burdekin River flood plume, Australia. Marine Pollution Bulletin 65, 236–248.

Bartley, R., Bainbridge, Z.T., Lewis, S.E., Kroon, F.J., Wilkinson, S.N., Brodie, J.E., Silburn, D.M., 2014. Relating sediment impacts on coral reefs to watershed sources, processes and management: A review. Science of the Total Environment 468, 1138–1153.

Beaman, R., 2010. Project 3DGBR: A high-resolution depth model for the Great Barrier Reef and Coral Sea. Marine and Tropical Sciences Research Facility (MTSRF) Project 2.5 i. 1a Final Report. Reef and Rainforest Research Centre, Cairns, Australia , pp13 & Appendix 1.

Belperio, A., 1983. Terrigenous sedimentation in the central Great Barrier Reef lagoon: a model from the Burdekin region. BMR Journal of Australian Geology and Geophysics 8, 179–190.

Blaise, S., Comblen, R., Legat, V., Remacle, J.F., Deleersnijder, E., Lambrechts, J., 2010. A discontinuous finite element baroclinic marine model on unstructured prismatic meshes. Part I: space discretization. Ocean Dynamics 60, 1371–1393.

Blaise, S., Deleersnijder, E., White, L., Remacle, J.F., 2007. Influence of the turbulence closure scheme on the finite-element simulation of the upwelling in the wake of a shallow-water island. Continental Shelf Research 27, 2329–2345.

de Brauwere, A., Gourgue, O., de Brye, B., Servais, P., Ouattara, N.K., Deleersnijder, E., 2014. Integrated modelling of faecal contamination in a densely populated river–sea continuum (Scheldt River and Estuary). Science of the Total Environment 468, 31–45.

Burchard, H., Bolding, K., Villarreal, M.R., 1999. GOTM, a general ocean turbulence model. Theory, implementation and test cases. Technical Report EUR 18745. European Commission.

Cabaço, S., Santos, R., Duarte, C.M., 2008. The impact of sediment burial and erosion on seagrasses: a review. Estuarine, Coastal and Shelf Science 79, 354–366.

Clark, T.R., Zhao, J.x., Roff, G., Feng, Y.x., Done, T.J., Nothdurft, L.D., Pandolfi, J.M., 2014. Discerning the timing and cause of historical mortality events in

modern porites from the Great Barrier Reef. Geochimica et Cosmochimica Acta 138, 57–80.

Comblen, R., Blaise, S., Legat, V., Remacle, J.F., Deleersnijder, E., Lambrechts, J., 2010. A discontinuous finite element baroclinic marine model on unstructured prismatic meshes. Part II: implicit/explicit time discretization. Ocean Dynamics 60, 1395–1414.

Devlin, M., Brodie, J., 2005. Terrestrial discharge into the Great Barrier Reef Lagoon: nutrient behavior in coastal waters. Marine Pollution Bulletin 51, 9–22.

Devlin, M., Petus, C., Collier, C., Zeh, D., McKenzie, L., 2013. Chapter 6: Seagrass and water quality impacts including a case study linking annual measurements of seagrass change against satellite water clarity data (Cleveland bay). Assessment of the Relative Risk of Water Quality to Ecosystems of the Great Barrier Reef: Supporting Studies. A report to the Department of the Environment and Heritage Protection, Queensland Government, Brisbane. TropWATER Report 13, 30.

DNRM, 2014. Streamflow discharge data provided by the State of Queensland (Department of Natural Resources and Mines). Available at http://www.dnrm.qld.gov.au/water/water-monitoring-and-data/portal, last accessed on October 22, 2014.

Egbert, G.D., Erofeeva, S.Y., 2002. Efficient inverse modeling of barotropic ocean tides. Journal of Atmospheric and Oceanic Technology 19, 183–204.

Elskens, M., Gourgue, O., Baeyens, W., Chou, L., Deleersnijder, E., Leermakers, M., de Brauwere, A., 2014. Modelling metal speciation in the Scheldt Estuary: combining a flexible-resolution transport model with empirical functions. Science of the Total Environment 476, 346–358.

Fabricius, K.E., 2005. Effects of terrestrial runoff on the ecology of corals and coral reefs: review and synthesis. Marine Pollution Bulletin 50, 125–146.

Fabricius, K.E., Death, G., Humphrey, C., Zagorskis, I., Schaffelke, B., 2013. Intra-annual variation in turbidity in response to terrestrial runoff on near-shore coral reefs of the Great Barrier Reef. Estuarine, Coastal and Shelf Science 116, 57–65.

Fabricius, K.E., Death, G., McCook, L., Turak, E., Williams, D.M., 2005. Changes in algal, coral and fish assemblages along water quality gradients on the inshore Great Barrier Reef. Marine Pollution Bulletin 51, 384–398.

Fabricius, K.E., Logan, M., Weeks, S., Brodie, J., 2014. The effects of river run-off on water clarity across the central Great Barrier Reef. Marine Pollution Bulletin .

Fielding, C.R., Trueman, J.D., Alexander, J., 2006. Holocene depositional history of the Burdekin River Delta of northeastern Australia: a model for a low-accommodation, highstand delta. Journal of Sedimentary Research 76, 411–428.

Flores, F., Hoogenboom, M.O., Smith, L.D., Cooper, T.F., Abrego, D., Negri, A.P., 2012. Chronic exposure of corals to fine sediments: lethal and sub-lethal impacts. PloS one 7, e37795.

Froidefond, J., Pujos, M., Andre, X., 1988. Migration of mud banks and changing coastline in French Guiana. Marine Geology 84, 19–30.

Geuzaine, C., Remacle, J.F., 2009. Gmsh: A 3-d finite element mesh generator with built-in pre-and post-processing facilities. International Journal for Numerical Methods in Engineering 79, 1309–1331.

Gourgue, O., Baeyens, W., Chen, M., de Brauwere, A., de Brye, B., Deleersnijder, E., Elskens, M., Legat, V., 2013. A depth-averaged two-dimensional sediment transport model for environmental studies in the Scheldt Estuary and tidal river network. Journal of Marine Systems 128, 27–39.

Harrington, L., Fabricius, K., Eaglesham, G., Negri, A., 2005. Synergistic effects of diuron and sedimentation on photosynthesis and survival of crustose coralline algae. Marine Pollution Bulletin 51, 415–427.

Hendy, E., Gagan, M., Lough, J., 2003. Chronological control of coral records using luminescent lines and evidence for non-stationary enso teleconnections in northeast Australia. The Holocene 13, 187–199.

Isdale, P., Stewart, B., Tickle, K., Lough, J., 1998. Palaeohydrological variation in a tropical river catchment: a reconstruction using fluorescent bands in corals of the Great Barrier Reef, Australia. The Holocene 8, 1–8.

Jackett, D.R., McDougall, T.J., Feistel, R., Wright, D.G., Griffies, S.M., 2006. Algorithms for density, potential temperature, conservative temperature, and the freezing temperature of seawater. Journal of Atmospheric and Oceanic Technology 23, 1709–1728.

Kärnä, T., Legat, V., Deleersnijder, E., 2013. A baroclinic discontinuous Galerkin finite element model for coastal flows. Ocean Modelling 61, 1–20.

Kärnä, T., Legat, V., Deleersnijder, E., Burchard, H., 2012. Coupling of a discontinuous Galerkin finite element marine model with a finite difference turbulence closure model. Ocean Modelling 47, 55–64.

King, B., McAllister, F., Wolanski, E., Done, T., Spagnol, S., 2001. River plume dynamics in the central Great Barrier Reef. Oceanographic Processes of Coral Reefs: Physical and Biological Links in the Great Barrier Reef , 145–159.

Kroon, F.J., Kuhnert, P.M., Henderson, B.L., Wilkinson, S.N., Kinsey-Henderson, A., Abbott, B., Brodie, J.E., Turner, R.D., 2012. River loads of suspended solids, nitrogen, phosphorus and herbicides delivered to the Great Barrier Reef lagoon. Marine Pollution Bulletin 65, 167–181.

Kuehl, S.A., Brunskill, G.J., Burns, K., Fugate, D., Kniskern, T., Meneghini, L., 2004. Nature of sediment dispersal off the Sepik River, Papua New Guinea: preliminary sediment budget and implications for margin processes. Continental Shelf Research 24, 2417–2429.

Kuhnert, P.M., Henderson, B.L., Lewis, S.E., Bainbridge, Z.T., Wilkinson, S.N., Brodie, J.E., 2012. Quantifying total suspended sediment export from the Burdekin River catchment using the loads regression estimator tool. Water Resources Research 48.

Lambeck, A., Woolfe, K., 2000. Composition and textural variability along the 10 m isobath, Great Barrier Reef: evidence for pervasive northward sediment transport. Australian Journal of Earth Sciences 47, 327–335.

Lambrechts, J., Humphrey, C., McKinna, L., Gourge, O., Fabricius, K., Mehta, A., Lewis, S., Wolanski, E., 2010. Importance of wave-induced bed liquefaction in the fine sediment budget of Cleveland Bay, Great Barrier Reef. Estuarine, Coastal and Shelf Science 89, 154–162.

Larcombe, P., Carter, R., 2004. Cyclone pumping, sediment partitioning and the development of the Great Barrier Reef shelf system: a review. Quaternary Science Reviews 23, 107–135.

Lewis, S.E., Olley, J., Furuichi, T., Sharma, A., Burton, J., 2014. Complex sediment deposition history on a wide continental shelf: Implications for the calculation of accumulation rates on the Great Barrier Reef. Earth and Planetary Science Letters 393, 146–158.

Lewis, S.E., Shields, G.A., Kamber, B.S., Lough, J.M., 2007. A multi-trace element coral record of land-use changes in the Burdekin River catchment, NE Australia. Palaeogeography, Palaeoclimatology, Palaeoecology 246, 471–487.

Liu, J., Xu, K., Li, A.e.a., Milliman, J., Velozzi, D., Xiao, S., Yang, Z., 2007. Flux and fate of Yangtze River sediment delivered to the East China Sea. Geomorphology 85, 208–224.

Lough, J.M., 2007. Tropical river flow and rainfall reconstructions from coral luminescence: Great Barrier Reef, Australia. Paleoceanography 22.

Lough, J.M., Lewis, S.E., Cantin, N.E., 2015. Freshwater impacts in the central Great Barrier Reef: 1648–2011. Coral Reefs , 1–13.

McCulloch, M., Fallon, S., Wyndham, T., Hendy, E., Lough, J., Barnes, D., 2003. Coral record of increased sediment flux to the inner Great Barrier Reef since European settlement. Nature 421, 727–730.

Milliman, J.D., Farnsworth, K.L., 2011. River discharge to the coastal ocean: a global synthesis. Cambridge University Press.

Muller, J., Wüst, R.A., Hearty, P.J., 2006. Sediment transport along an artificial shoreline: The Strand, Townsville, NE-Queensland, Australia. Estuarine, Coastal and Shelf Science 66, 204–210.

Orpin, A., Ridd, P., Stewart, L., 1999. Assessment of the relative importance of major sediment transport mechanisms in the central Great Barrier Reef lagoon. Australian Journal of Earth Sciences 46, 883–896.

Orpin, A.R., Brunskill, G., Zagorskis, I., Woolfe, K., 2004. Patterns of mixed siliciclastic–carbonate sedimentation adjacent to a large dry-tropics river on the central Great Barrier Reef shelf, Australia. Australian Journal of Earth Sciences 51, 665–683.

Petus, C., Collier, C., Devlin, M., Rasheed, M., McKenna, S., 2014. Using MODIS data for understanding changes in seagrass meadow health: A case study in the Great Barrier Reef (Australia). Marine environmental research 98, 68–85.

Pham Van, C., Deleersnijder, E., Bousmar, D., Soares-Frazão, S., 2014. Simulation of flow in compound open-channel using a discontinuous galerkin finite-element method with Smagorinsky turbulence closure. Journal of Hydro-environment Research 8, 396–409.

Pringle, A.W., 1986. Causes and effects of changes in fluvial sediment yield to the north-east Queensland coast, Australia. Department of Geography, James Cook University of North Queensland Townsville.

Puig, P., Ogston, A., Mullenbach, B., Nittrouer, C., Sternberg, R., 2003. Shelf-to-canyon sediment-transport processes on the Eel continental margin (northern California). Marine Geology 193, 129–149.

Restrepo, J.D., Zapata, P., Díaz, J.M., Garzón-Ferreira, J., García, C.B., 2006. Fluvial fluxes into the Caribbean Sea and their impact on coastal ecosystems: The Magdalena River, Colombia. Global and Planetary Change 50, 33–49.

Roff, G., Clark, T.R., Reymond, C.E., Zhao, J.x., Feng, Y., McCook, L.J., Done, T.J., Pandolfi, J.M., 2013. Palaeoecological evidence of a historical collapse of corals at Pelorus Island, inshore Great Barrier Reef, following European settlement. Proc R Soc B: Biol. Sci. 280, rspb20122100.

Saha, S., Moorthi, S., Pan, H.L., Wu, X., Wang, J., Nadiga, S., Tripp, P., Kistler, R., Woollen, J., Behringer, D., et al., 2010. The NCEP climate forecast system reanalysis. Bulletin of the American Meteorological Society 91, 1015–1057.

Smagorinsky, J., 1963. General circulation experiments with the primitive equations: I. the basic experiment*. Monthly weather review 91, 99–164.

Syvitski, J.P., Vörösmarty, C.J., Kettner, A.J., Green, P., 2005. Impact of humans on the flux of terrestrial sediment to the global coastal ocean. Science 308, 376–380.

Thomas, C.J., Lambrechts, J., Wolanski, E., Traag, V.A., Blondel, V.D., Deleersnijder, E., Hanert, E., 2014. Numerical modelling and graph theory tools to study ecological connectivity in the Great Barrier Reef. Ecological Modelling 272, 160–174.

Weber, M., de Beer, D., Lott, C., Polerecky, L., Kohls, K., Abed, R.M., Ferdelman, T.G., Fabricius, K.E., 2012. Mechanisms of damage to corals exposed to sedimentation. Proceedings of the National Academy of Sciences 109, E1558–E1567.

Weber, M., Lott, C., Fabricius, K., 2006. Sedimentation stress in a scleractinian coral exposed to terrestrial and marine sediments with contrasting physical, organic and geochemical properties. Journal of Experimental Marine Biology and Ecology 336, 18–32.

Weeks, S., Werdell, P.J., Schaffelke, B., Canto, M., Lee, Z., Wilding, J.G., Feldman, G.C., 2012. Satellite-derived photic depth on the Great Barrier Reef: spatio-temporal patterns of water clarity. Remote Sensing 4, 3781–3795.

Wolanski, E., Elliott, M., 2015. Estuarine Ecohydrology. II ed., Elsevier, Amsterdam. In press.

Wolanski, E., Jones, M., 1981. Physical properties of Great Barrier Reef lagoon waters near Townsville. I. Effects of Burdekin River floods. Marine and Freshwater Research 32, 305–319.

Wolanski, E., Richmond, R.H., Davis, G., Bonito, V., 2003. Water and fine sediment dynamics in transient river plumes in a small, reef-fringed bay, Guam. Estuarine, Coastal and Shelf Science 56, 1029–1040.

Wolanski, E., van Senden, D., 1983. Mixing of Burdekin River flood waters in the Great Barrier Reef. Marine and Freshwater Research 34, 49–63.

Woolfe, K., Larcombe, P., 1998. Terrigenous sediment accumulation as a regional control on the distribution of reef carbonates. Reefs and carbonate platforms in the Pacific and Indian Oceans , 295–310.

Xue, Z., Liu, J.P., DeMaster, D., Van Nguyen, L., Ta, T.K.O., 2010. Late Holocene evolution of the Mekong subaqueous delta, southern Vietnam. Marine Geology 269, 46–60.